Supplementary Information to:

Impact of iron- and/or sulfate-reduction on a *cis*-1,2-dichloroethene and vinyl chloride respiring bacterial consortium: experiments and model-based interpretation

Alexandra Murray[a], Julien Maillard[b], Massimo Rolle[a*], Mette M. Broholm[a], and Christof Holliger[b]

[a]Department of Environmental Engineering, Technical University of Denmark, Kgs. Lyngby, DK-2800, Denmark

[b]Laboratory for Environmental Biotechnology, ENAC-IIE, Ecole Polytechnique Fédérale de Lausanne, 1015 Lausanne, Switzerland

1. Medium composition and batch configuration

Table S1: Medium composition

Compound	Value	Unit
$K_2HPO_4 \cdot 3H_2O$	3.78	*mmol/L medium*
$NaH_2PO_4 \cdot 2H_2O$	1.28	
NH_4HCO_3	5.58	
$NaHCO_3$	44.39	
$Na_2S \cdot 9H_2O$	0.01	
$CaCl_2 \cdot 2H_2O$	0.75	
$MgCl_2 \cdot 6H_2O$	0.50	
Ferric citrate	4.90	
Sodium sulfate	4.90	
Acetate	1.96	
EDTA	1.70	*µmol/L medium*
$FeCl_2 \cdot 4H_2O$	10.06	
$MnCl_2 \cdot 4H_2O$	0.51	
$CoCl_2 \cdot 6H_2O$	0.80	
$ZnCl_2$	0.51	
$CuCl_2 \cdot 2H_2O$	0.01	
$AlCl_3 \cdot 6H_2O$	0.04	
H_3BO_3	0.10	
$Na_2MoO_4 \cdot 2H_2O$	0.17	
$NiCl_2 \cdot 6H_2O$	0.10	
Biotin	0.20	*nmol/L medium*
P-aminobenzoate	1.57	
Pantothenate	0.21	
Folic acid	0.04	
Lipoic acid	0.24	
Pyridoxine	0.59	
Nicotinamide	4.50	
Thiamine HCl	100.00	*µg/L medium*
Riboflavine	50.00	
Cyanocobalamin	50.00	
Resazurin	0.01	*g/L medium*
Ti(III)-citrate	5 drops, approx. 100 µL	

Point	Inoculation Ratio		
	OHRB : FeRB : SRB		
1	1	0	0
2	1	0	10^{-2}
3	1	10^{-2}	0
4	1	10^{-2}	10^{-2}

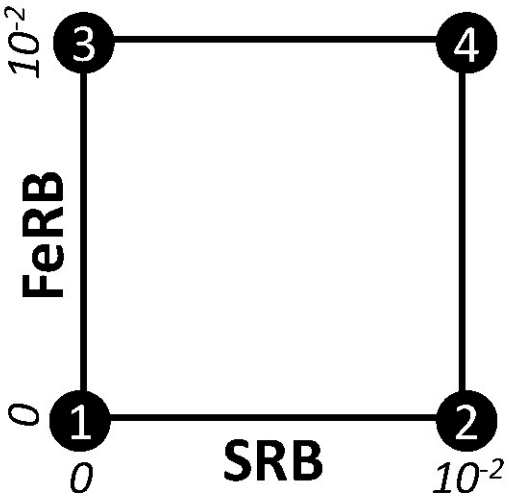

Figure S1: Schematic of the batch inocula configurations, where each numbered circle on the experimental domain is one of the batch bottles. The ratios in the table correspond to the number of cells of each inoculum added to the batch.

2. Molecular method details

Universal qPCR for inocula cell count determination

The universal primers 338f (5'-ACTCCTACGGGAGGCAGCAG-3') (Jossi et al., 2006) and 518r (5'-ATTACCGCGGCTGCTGG-3') (Muyzer et al., 1993) were used. The qPCR thermocycling prorgam used for the inocula cell count analysis was the standard protocol (Murray et al., 2019) with an annealing temperature of 62°C and acquisition temperature of 72°C.

Terminal Restriction Fragment Length Polymorphism (T-RFLP) analysis

Anaerobic culture samples were incubated for 5 min in boiling water for cell lysis. The samples were then diluted 100-fold in sterile ddH_2O to prevent PCR inhibition and used as template for a two-step non-saturating PCR approach as described below.

First step PCR amplification of 16S rDNA genes. A 5-µL reaction mixture typically consisted of 1 µL of 5× MyFi Reaction Buffer (bioline, LabGene Scientific, Châtel-St-Denis, Switzerland), 0.2 µL of 8f universal primer (5'-AGAGTTTGATCCTGGCTCAG-3') and 518r universal primer (5'-GTATTACCGCGGCTGCTGG-3'), 2.4 µL of sterile ddH_2O, 0.2 µL of MyFi DNA Polymerase (bioline) and 1 µL of lysed and diluted culture samples. The PCR program was the following: 1 min of denaturation at 95°C, 20 cycles of 15 s of denaturation at 95°C, 15 s of primer annealing at 56°C and 15 s of elongation at 72°C. The complete reaction volume was used as template for the second step PCR.

Second step PCR amplification of 16S rDNA genes. A 45-µL reaction mixture typically consisted of 5 µL of 10× Taq Buffer (PeqLab, Axonlab, Baden-Dättwill, Switzerland), 23 µL of sterile ddH_2O, 1.5 µL of 10 mM dNTPs, 10 µL of enhancer solution (PeqLab), 2.5 µL of FAM-labeled 8f primer and 2.5 µL of 518r primer, and 0.5 µL of Taq DNA Polymerase (PeqLab). The reaction

mixture was added to tube resulting from the first step PCR. The PCR program was the following: 10 min denaturation at 95°C, 20 cycles of 1 min denaturation at 95°C, 45 s of primer annealing at 56°C and 1 min of elongation at 72°C, followed by 5 min final extension at 72°C.

Aliquots of 5 µL of products resulting from the second step PCR were analyzed by agarose gel electrophoresis according to standard protocols before the rest of PCR products were purified using the MSB Spin PCRapace kit (Stratec, Chemie Brunschwig AG, Basel, Switzerland) according to the manufacturer's instructions. The PCR products were eluted in 20 µL of elution buffer (Stratec) and quantified with the NanoDrop spectrophotometer (ND-1000, Witec, Sursee, Switzerland).

Digestion with *Alu*I restriction enzyme. The reaction mixture typically consisted of 50 ng of DNA (purified PCR products), 1 µL of Restriction Buffer B (Promega AG, Dübendorf, Switzerland), 0.12 µL of *Alu*I restriction enzyme (Promega) and sterile ddH_2O (ad 10 µL). The reaction was incubated 3 h at 37°C.

Samples for T-RFLP analysis were prepared as follows: 1 µL of digested DNA, 0.5 µL of GeneScan 600 LIZ Dye Standard (Fisher Scientific, Illkirch, France) and 8.5 µL of HiDiTM Formamide (Life Technologies, Thermo Fisher Scientific AG, Reinach, Switzerland). Samples were mixed by vortexing, incubated 2 min at 95°C, incubated on ice for 3 min and run in the ABI PRISM 3100 Genetic Analyzer 3130xl (Thermo Fisher Scientific) as previously described (Buttet et al., 2013).

T-RFLP data analysis

The T-RFLP output data was treated by only selecting fragments of 50-500 bp with a height greater than 100 and that composed greater than 2% of each sample. Fragments of length 126-128 were attributed to *Dehalococcoides* spp., fragments of length 205-206 were attributed to the added

Desulfovibrio vulgaris, fragments of length 208-210 were attributed to the endogenous *Desulfovibrio vulgaris* population, and fragments of length 234 were attributed to both the added and endogenous *Shewanella oneidensis* populations. Only these fragments were selected for further analysis. The number of fragments attributable to each species in each sample were divided by the number of 16S rRNA gene copies per genome for each species – 1 gene copy $cell^{-1}$ for *Dehalococcoides* (Ritalahti et al., 2006), 5 gene copies $cell^{-1}$ for *Desulfovibrio vulgaris* (Heidelberg et al., 2004), and 9 gene copies $cell^{-1}$ for *Shewanella oneidensis* (Heidelberg et al., 2002) – and presented as relative cell proportions. Fragments not attributable to these guilds were on average 33% of each sample. Fragments of length 69 were sometimes highly abundant and were attributed to *Wolinella succinogenes*, which respires fumarate with hydrogen as an electron donor (Kröger et al., 2002). Because fumarate is not a media component, the metabolism of *W. succinogenes* is unknown, and therefore not included in the selected fragment set. Fragments of length 237 were consistently present at low relative abundance. These fragments were attributed to *Aminobacterium colombiense*, a fermentative bacterium (Chertkov et al., 2010) and established as distinct from *S. oneidensis* at fragment length 234.

3. Modeling approach

An in-depth description of the modeling tool used in this study and its capability to integrate microbial activity, mass transfer, and geochemical processes can be found in Murray et al. (2019). The equations presented in this section were used in the model to describe mass transfer, aqueous speciation, biotic Fe(III) and sulfate reduction, abiotic Fe(III) reduction, and $FeS_{(s)}$ precipitate formation.

Mass transfer: The following equations describe the kinetic movement of volatile compounds between the phases. Equations S1, S2, and S3 are a set of ordinary differential equations that describe the change in concentration in each phase, and Equations S4 and S5 describes the movement of mass from one phase to another:

$$\frac{dC_{i,aq}}{dt} = \frac{\left(\frac{dn_i}{dt}\right)_{gas-aq}}{V_{aq}} + \frac{\left(\frac{dn_i}{dt}\right)_{org-aq}}{V_{aq}} \quad (S1)$$

$$\frac{dC_{i,org}}{dt} = \frac{-\left(\frac{dn_i}{dt}\right)_{org-aq}}{V_{org}} + \frac{-\left(\frac{dn_i}{dt}\right)_{org-gas}}{V_{org}} \quad (S2)$$

$$\frac{dC_{i,gas}}{dt} = \frac{-\left(\frac{dn_i}{dt}\right)_{gas-aq}}{V_{gas}} + \frac{\left(\frac{dn_i}{dt}\right)_{org-aq}}{V_{gas}} \quad (S3)$$

$$\left(\frac{dn_i}{dt}\right)_{org-aq} = V_{aq}(C_{i,aq}^{eq} - C_{i,aq})\left(\frac{\kappa_{i,org-aq} \cdot A}{V_{org}}\right) \quad (S4)$$

$$\left(\frac{dn_i}{dt}\right)_{org-gas} = V_{gas}(C_{i,gas}^{eq} - C_{i,gas})\left(\frac{\kappa_{i,org-gas} \cdot A}{V_{org}}\right) \quad (S5)$$

where $dC_{i,p}/dt$ [mol L^{-1} s^{-1}] is the change in concentration for compound i in phase p, V_p [L] is the volume of phase p, dn_i/dt [mol s^{-1}] is the total change in moles between phases for the compound, $C_{i,p}$ [M] and $C^{eq}_{i,p}$ [M] are the concentration and equilibrium concentration of compound i in phase

p, $\kappa_{i,org\text{-}aq}$ [dm s^{-1}] and $\kappa_{i,org\text{-}gas}$ [dm s^{-1}] are the mass transfer coefficients for the compound i, and A [dm^2] is the cross-sectional area of the phase interface.

Aqueous speciation of Fe(III)-citrate: The Fe(III) substrate speciation was computed through the IPhreeqc coupling module according to the following speciation reactions:

Table S2. Fe(III)-citrate speciation reactions

Reaction	Log(k)
$Fe^{3+} + Citrate^{3-} + H_2O \rightarrow FeCitrateOH^- + H^+$	9.98[a]
$Fe^{3+} + Citrate^{3-} \rightarrow FeCitrate$	12.55[b]
$Fe^{3+} + 2Citrate^{3-} + H_2O \rightarrow FeCitrate_2OH^{4-} + H^+$	13.42[a]
$Fe^{3+} + Citrate^{3-} + H^+ \rightarrow FeCitrateH^+$	19.8[b]
$Fe^{3+} + 2Citrate^{3-} + 2H^+ \rightarrow FeCitrate_2H_2^-$	26.46[a]

[a]Reaction and log(k) as described in Liu et al. (2001)
[b]Reaction and log(k) from the PHREEQC Minteq database

Fe(III) and sulfate reduction, bacterial growth: Fe(III) reduction by FeRB and sulfate reduction by SRB and SRBi were modeled using double Monod kinetics (Equation S6). Bacterial growth and decay for all guilds, including OHRB, were modeled by Equation S7. Fe(III) reduction by SRB and SRBi was modeled by Equation S8 (Elias et al., 2004).

$$\frac{dC_{aq,EA}}{dt} = -k_{max}X\left(\frac{C_{aq,ED}}{C_{aq,ED} + K_{S,ED}}\right)\left(\frac{C_{aq,EA}}{C_{aq,EA} + K_{S,EA}}\right) \quad (S6)$$

$$\frac{dX}{dt} = Y_{EA}\frac{dC_{aq,EA}}{dt} - k_dX \quad (S7)$$

$$\frac{dC_{aq,Fe(III)}}{dt} = k_{FeBio}C_{Fe(III),Bio} \quad (S8)$$

In the equations above, $dC_{aq,EA}/dt$ [mol L^{-1} h^{-1}] is the change in electron acceptor in the aqueous phase due to bacterial processes, $C_{aq,ED}$ and $C_{aq,EA}$ [µM] are the aqueous concentration of electron donor and acceptor, k_{max} [mol cell^{-1} s^{-1}] is the maximum specific reduction rate, X [cells L^{-1}] is the biomass concentration, t [s] is time, $K_{S,ED}$ and $K_{S,EA}$ [M] are the half-saturation constants for the

electron donor and acceptor, Y_{EA} [cells mol^{-1}] is the biomass yield on the electron acceptor, k_d [s^{-1}] is the linear decay coefficient, and k_{FeBio} [s^{-1}] is the first-order rate constant. Hydrogen was the electron donor for all guilds. For SRB and SRBi reduction of Fe(III), growth was modeled to not occur (Y_{EA} = 0) (Elias et al., 2004; Park et al., 2008).

Abiotic Fe(III) reduction: Sulfide species, a product of bacterial sulfate reduction, are capable of reducing Fe(III) to Fe(II) (Equation S9) (Poulton et al., 2004; Rickard and Luther, 2007). The rate of this process has been determined to be first order with respect to Fe(III) and 0.5 order with respect to sulfide (Poulton et al., 2004):

$$2Fe^{3+} + HS^{-} \rightarrow 2Fe^{2+} + S^{0} + H^{+} \qquad (S9)$$

$$\frac{dC_{Fe(II)}}{dt} = k_{FeAbio} C_{Fe(III)} C_{S(-II)}{}^{0.5} \qquad (S10)$$

where k_{FeAbio} [L$^{0.5}$ mol$^{-0.5}$ s^{-1}] is the kinetic rate constant for Fe(II) production as a result of abiotic Fe(III) reduction.

FeS(s) precipitate formation: Sulfide species also react with Fe(II) to form iron-sulfide precipitates. Amorphous FeS(s) production was modelled via the stoichiometric reaction in Equation S11, and proceeded at equilibrium (Jakobsen, 2007):

$$Fe^{2+} + HS^{-} \rightarrow FeS_{(s)} + H^{+} \qquad (S11)$$

4. Model parameters

Table S3: Model parameters, where org = organic phase, aq = aqueous phase, gas = gaseous phase, CE = chlorinated ethenes, H2 = hydrogen, cDCE = cis-1,2-dichloroethene, VC = vinyl chloride, Eth = ethene, OHRB = organohalide-respiring bacteria, SRB = sulfate-reducing bacteria, SRBi = indigenous sulfate-reducing bacteria, FeRB = Fe(III)-reducing bacteria, Fe3 = Fe(III), SO4 = sulfate.

Parameter	Description	Value	[unit]
$\kappa_{org\text{-}aq,CE}$	Mass transfer rate for chlorinated ethenes across the org-aq phase boundary	1.5 [a]	dm s^{-1}
$\kappa_{org\text{-}gas,CE}$	Mass transfer rate for chlorinated ethenes across the org-gas phase boundary	0.47 [a]	dm s^{-1}
$\kappa_{org\text{-}aq,H2}$	Mass transfer rate for hydrogen across the org-aq phase boundary	0.1 [b]	dm s^{-1}
$\kappa_{org\text{-}gas,H2}$	Mass transfer rate for hydrogen across the org-gas phase boundary	0.47 [b]	dm s^{-1}
$K_{org\text{-}aq,cDCE}$	cDCE hexadecane-water partition coefficient	87.096 [c]	$L_{aq}\ L_{hex}^{-1}$
$K_{aq\text{-}gas,cDCE}$	cDCE air-water partition coefficient	0.2454 [d]	$L_{aq}\ L_{gas}^{-1}$
$K_{org\text{-}aq,VC}$	VC octanol-water partition coefficient	33.11 [e]	$L_{aq}\ L_{oct}^{-1}$
$K_{aq\text{-}gas,VC}$	VC air-water partition coefficient	1.5142 [d]	$L_{aq}\ L_{gas}^{-1}$
$K_{org\text{-}aq,Eth}$	Ethene hexadecane-water partition coefficient	16.9824 [c]	$L_{aq}\ L_{oct}^{-1}$
$K_{aq\text{-}gas,Eth}$	Ethene air-water partition coefficient	8.7444 [f]	$L_{aq}\ L_{gas}^{-1}$
$K_{org\text{-}aq,H2}$	H_2 octanol-water partition coefficient	1 [b]	$L_{aq}\ L_{oct}^{-1}$
$K_{aq\text{-}gas,H2}$	H_2 air-water partition coefficient	56.18	$L_{aq}\ L_{gas}^{-1}$
$K_{S,OHRB,cDCE}$	Half-velocity constant for OHRB for cDCE	4×10^{-7} [g]	M
$K_{CI,OHRB,cDCE}$	Competitive inhibition constant for OHRB for VC	4×10^{-7} [g]	M
$K_{S,OHRB,VC}$	Half-velocity constant for OHRB for VC	6×10^{-4} [g]	M
$K_{S,OHRB,H2}$	Half-velocity constant for OHRB for H_2	7×10^{-9} [h]	M
$K_{S,FeRB,H2}$	Half-velocity constant for FeRB for H_2	1.39×10^{-7} [i]	M
$K_{S,SRB,SO4}$	Half-velocity constant for SRB for SO_4^{2-}	3×10^{-3} [j,o]	M
$K_{S,SRB,H2}$	Half-velocity constant for SRB for H_2	1.4×10^{-6} [j]	M
k_d	First order decay constant (all guilds)	0.024 [k]	d^{-1}
k_{FeBio}	First-order rate constant for Fe(III) red. by SRB	2.5×10^{-3} [l]	s^{-1}
$Y_{OHRB,cDCE}$	Yield on cDCE, OHRB	1.32×10^{14} [g]	Cell mol_{cDCE}^{-1}
$Y_{OHRB,VC}$	Yield on VC, OHRB	1.32×10^{14} [g]	Cell mol_{VC}^{-1}
$Y_{FeRB,Fe3}$	Yield on electron acceptor, FeRB	1.31×10^{14} [m]	Cell mol_{Fe3}^{-1}
$Y_{SRB,H2}$	Yield on electron donor, SRB	0.025 [j]	$mol_{bio}\ mol_{H2}^{-1}$
$Y_{SRB,Fe3}$	Yield on Fe(III), SRB	0 [n]	Cell mol_{Fe3}^{-1}
k_{FeAbio}	Rate constant for abiotic Fe(III) red. by S(-II)	3.64×10^{-4} [o]	$L^{0.5}\ mol^{-0.5}\ s^{-1}$
R	Universal gas constant	8.0206×10^{-2}	L atm K^{-1} mol^{-1}
V_{aq}	Initial volume of the aqueous base media (initial volume of the aqueous phase excluding inocula)	60	mL

Parameter	Description	Value	[unit]
V_{org}	Volume of the organic phase	2	mL
V_{gas}	Initial volume of the gas phase (excluding inocula)	63	mL
$V_{S,aq}$	Sample volume of the aqueous phase	1.0	mL
$V_{S,gas}$	Sample volume of the gas phase	1.5	mL
A	Bottle cross sectional area, area of phase interface	0.181	dm^2
$X_{0,OHRB}$	Initial concentration of OHRB cells	8.81×10^8	Cell L^{-1}
$X_{0,FeRBi}$	Initial concentration of FeRBi cells	$X_{0,OHRB} \times 0.25\%$ [p]	Cell L^{-1}
$X_{0,SRBi}$	Initial concentration of SRBi cells	$X_{0,OHRB} \times 0.25\%$ [p]	Cell L^{-1}
$X_{0,FeRB}$	Initial concentration of FeRB cells	$X_{0,OHRB} \times 1\%$	Cell L^{-1}
$X_{0,SRB}$	Initial concentration of SRB cells	$X_{0,OHRB} \times 1\%$	Cell L^{-1}
$k_{max,FeRB}$	Maximum Fe(III) utilization rate for all FeRB	1.0×10^{-18} [p]	mol_{Fe3} $cell^{-1}$ s^{-1}
$k_{max,SRB}$	Maximum sulfate utilization rate for all SRB	7.0×10^{-18} [p]	mol_{SO4} $cell^{-1}$ s^{-1}
$t_{lag,SRBi}$	Lag time for the SRBi guild	3 [p]	d

[a] Determined using information in (Aeppli et al., 2009) and method in (Buttet et al., 2018), [b] (Aeppli et al., 2009), [c] (Abraham et al., 1990), [d] (Warneck, 2007), [e] (Gossett et al., 1983), [f] (Sander, 2015), [g] (Schneidewind et al., 2014) and references therein, including (Yu and Semprini, 2004) (range given for $K_{S,OHRB,cDCE}$ = 0.0018-0.0370 mM, $K_{S,OHRB,VC}$ = 0.0038-0.0378 mM, $Y_{OHRB} = 7.76 \times 10^8$ -2.86×10^{12} cell $mmol^{-1}$), [h] (Cupples et al., 2004), [i] (Malaguerra et al., 2011), [j] (Noguera et al., 1998), [k] (Yu and Semprini, 2004), [l] Representative of rates: (Elias et al., 2004; Lovley et al., 1993; Park et al., 2008; Zhou et al., 2017), [m] (Liu et al., 2001), [n] (Elias et al., 2004), [o] (Murray et al., 2019), [p] estimated value based on forward fitting used in all batch simulations

5. Duplicate batch data and simulations

Data for T-RFLP and sulfate is presented here for all batches and their duplicates. There is evident agreement between the duplicates for each of the types of data.

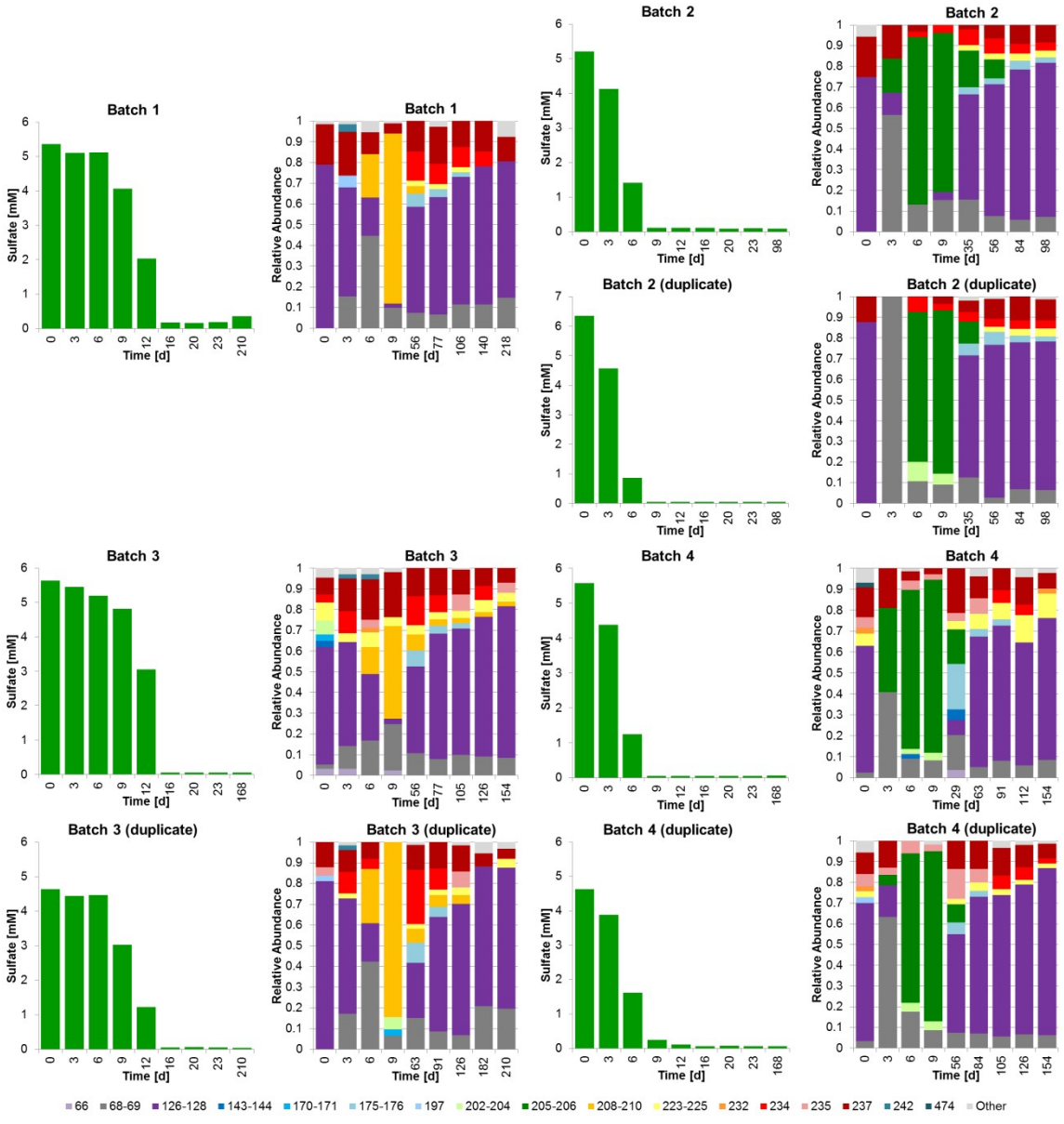

Figure S2: Sulfate and relative abundance data for each of the interpreted datasets and their duplicates. The duplicate for Batch 1 was suspected to have a leaky septum seal and was not included in the analysis.

The chloride curves of the three batches with duplicates also demonstrate this reproducibility. All batches with duplicates were able to be simulated with the same kinetic variables. In Batches 3 and 4, the duplicates varied only in the lag time; the chlorinated ethene degradation curves are superimposable when the lag time is accounted for. The slight differences in the shape of the simulated chloride evolution curves between the duplicates in Batches 3 and 4 is due to the effects of consecutive sample removal – if samples are removed in the same way in both batches, but chloride is produced later in the time series in the batch duplicate with a longer lag time, the measured/simulated chloride concentration at the end of the time series will be greater, as the same amount of chloride is produced in a smaller aqueous volume.

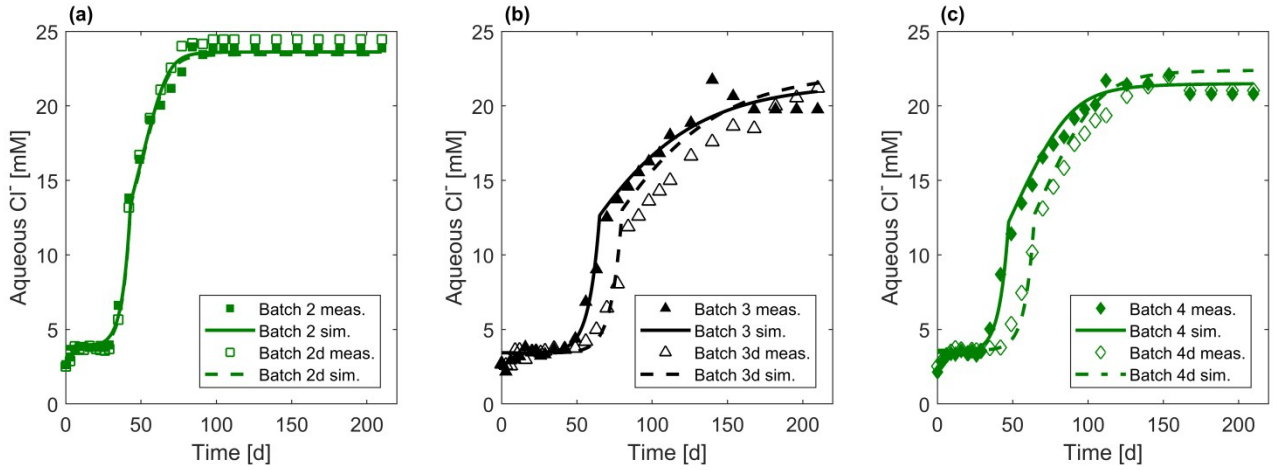

Figure S3: Duplicate chloride evolution curves for Batch 2 (Panel a), Batch 3 (Panel b), and Batch 4 (Panel c)

The lag information for each batch is as follows:

- Batch 1 = 20 d
- Batch 2 & 2d = 9 d
- Batch 3 = 20 d, Batch 3d = 35 d
- Batch 4 = 9 d, Batch 4d = 26 d

Batch 3 is used as an example for the chemical and biological data and simulations in the main document. The remainder of all batch data and simulations and their duplicates are included in the following figures:

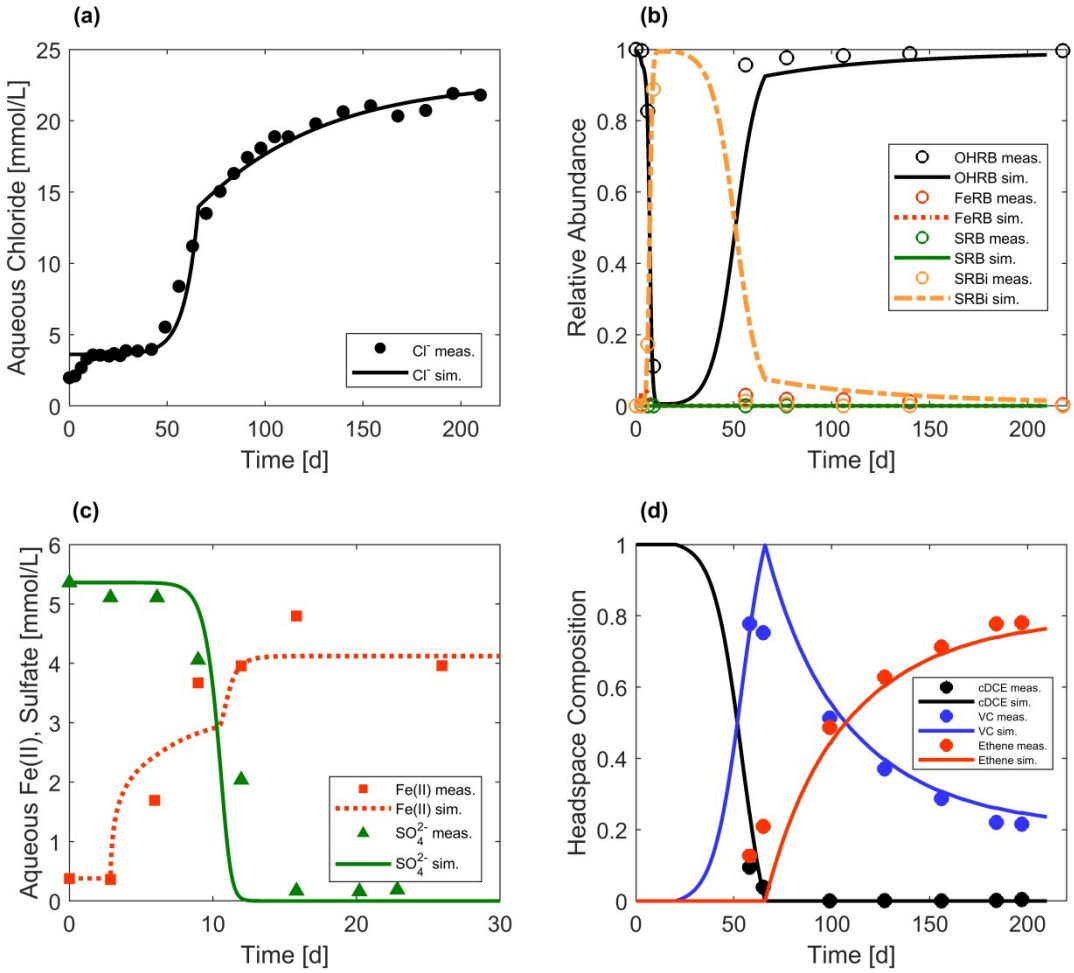

Figure S4: Batch 1 data and simulations for aqueous chloride concentration (a), microbial community relative abundance (b), aqueous Fe(II) and sulfate concentrations(c), and relative headspace composition of chlorinated ethenes (d). Time axis is scaled for panel (c) to best display the change in concentration that occurs at the beginning of the time series.

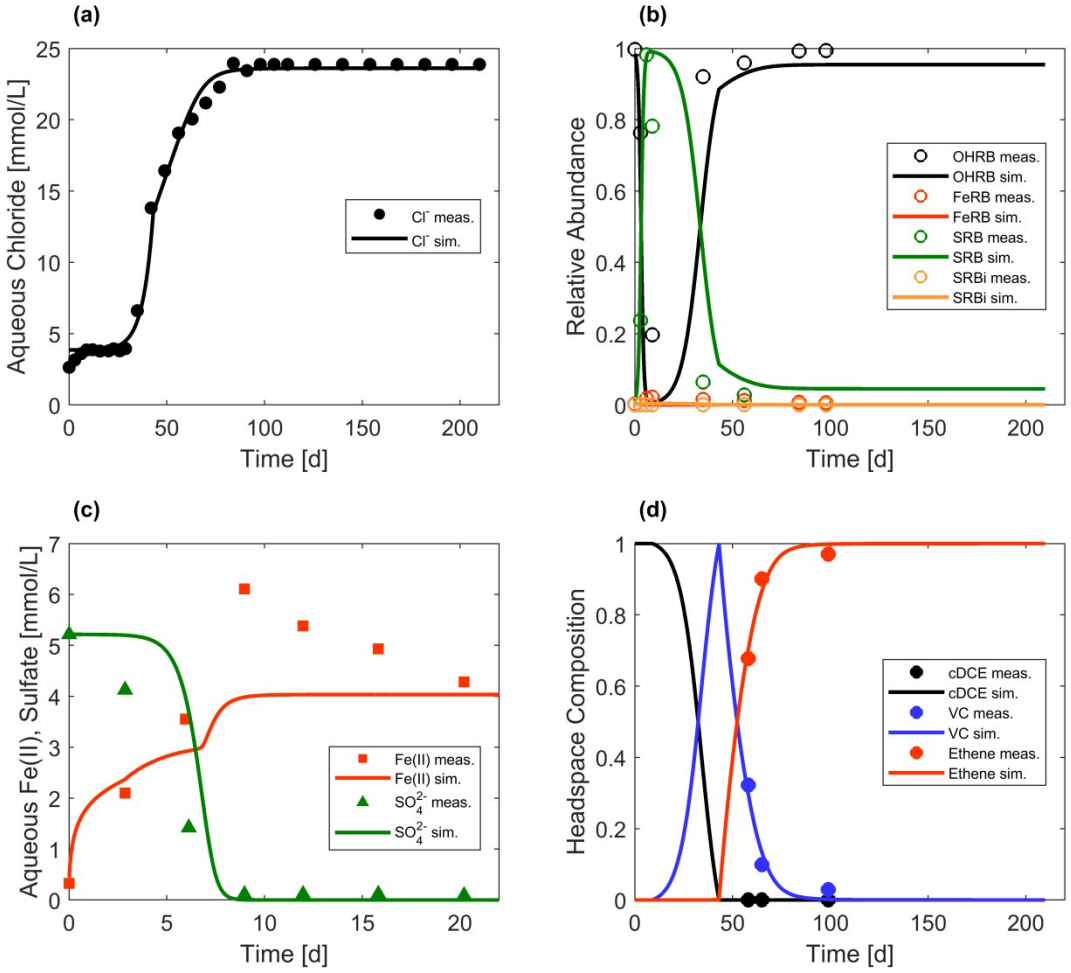

Figure S5: Batch 2 data and simulations for aqueous chloride concentration (a), microbial community relative abundance (b), aqueous Fe(II) and sulfate concentrations(c), and relative headspace composition of chlorinated ethenes (d). Time axis is scaled for panel(c) to best display the change in concentration that occurs at the beginning of the time series.

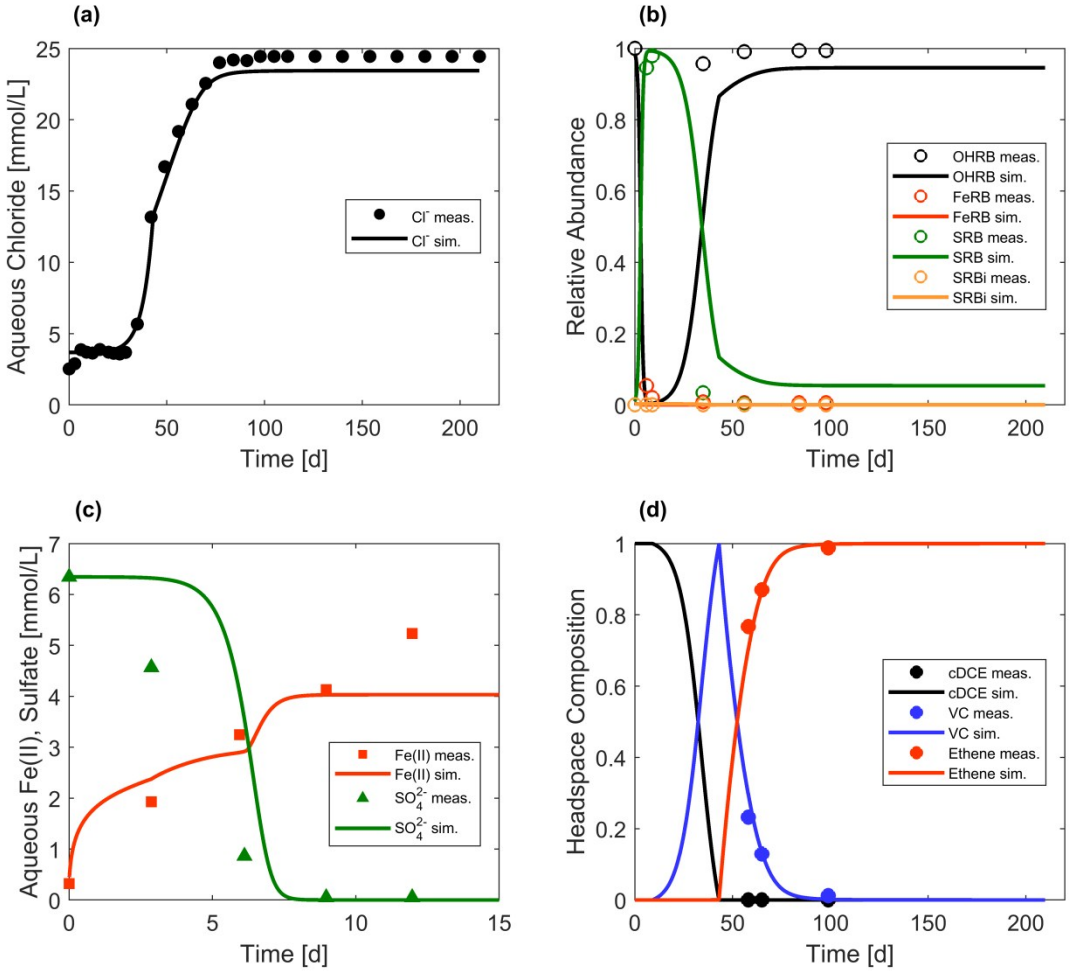

Figure S6: Batch 2d data and simulations for aqueous chloride concentration (a), microbial community relative abundance (b), aqueous Fe(II) and sulfate concentrations(c), and relative headspace composition of chlorinated ethenes (d). Time axis is scaled for panel(c) to best display the change in concentration that occurs at the beginning of the time series.

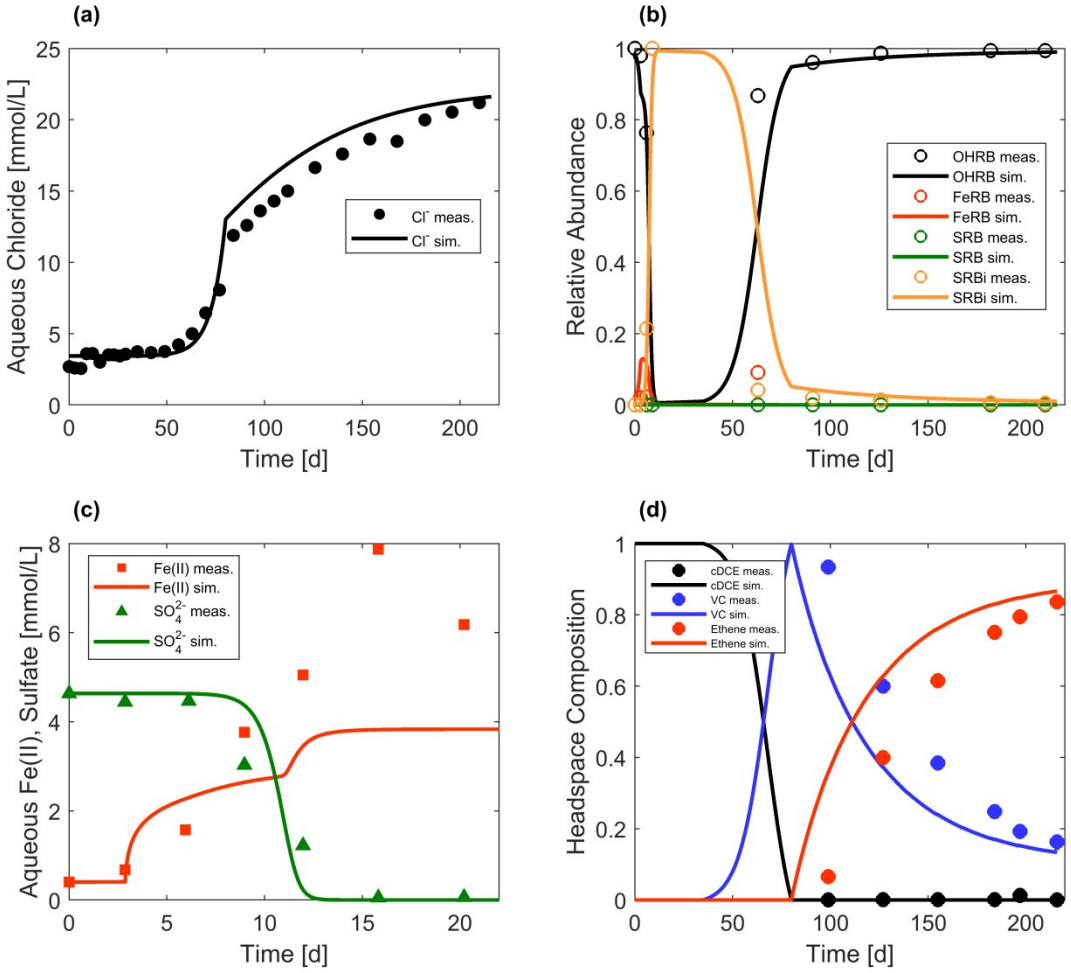

Figure S7: Batch 3d data and simulations for aqueous chloride concentration (a), microbial community relative abundance (b), aqueous Fe(II) and sulfate concentrations(c), and relative headspace composition of chlorinated ethenes (d). Time axis is scaled for panel(c) to best display the change in concentration that occurs at the beginning of the time series.

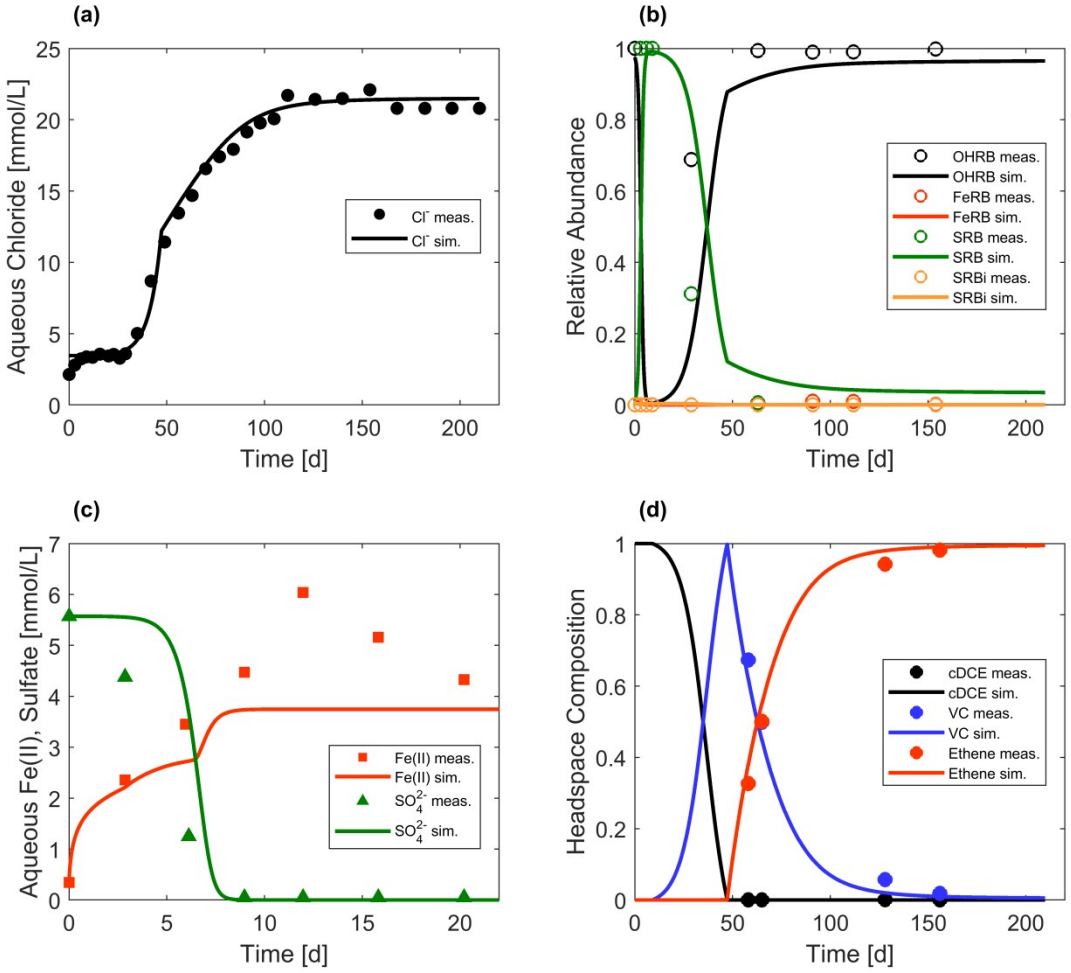

Figure S8: Batch 4 data and simulations for aqueous chloride concentration (a), microbial community relative abundance (b), aqueous Fe(II) and sulfate concentrations(c), and relative headspace composition of chlorinated ethenes (d). Time axis is scaled for panel(c) to best display the change in concentration that occurs at the beginning of the time series.

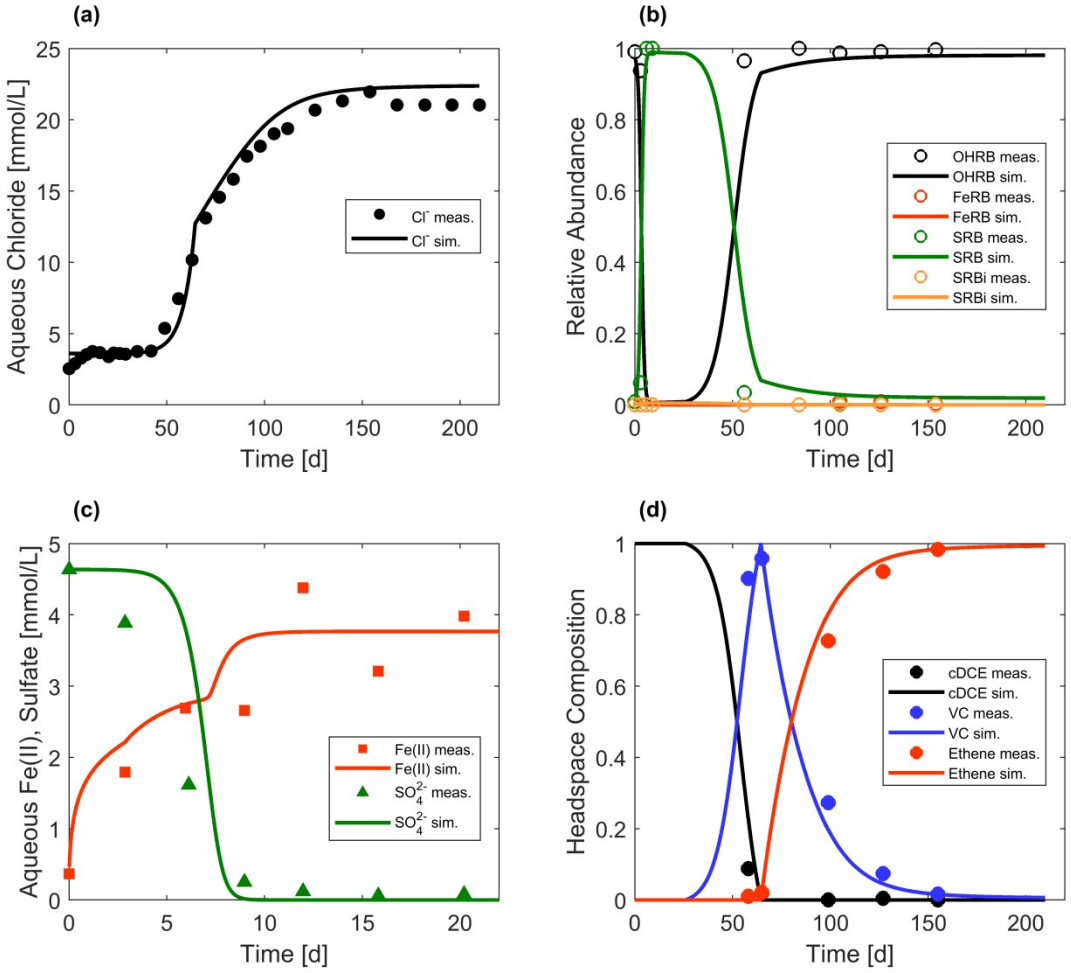

Figure S9: Batch 4d data and simulations for aqueous chloride concentration (a), microbial community relative abundance (b), aqueous Fe(II) and sulfate concentrations(c), and relative headspace composition of chlorinated ethenes (d). Time axis is scaled for panel(c) to best display the change in concentration that occurs at the beginning of the time series.

6. NRMSE for all simulations

Data	Batch	NRMSE
Chloride	1	0.039
Fe(II)	1	0.498
Sulfate	1	0.144
OHRB	1	0.108
FeRB	1	0.767
SRBi	1	0.119
cDCE	1	0.606
VC	1	0.160
Ethene	1	0.147

Data	Batch	NRMSE	Batch	NRMSE
Chloride	2	0.031	2d	0.038
Fe(II)	2	0.331	2d	0.492
Sulfate	2	0.165	2d	0.192
OHRB	2	0.152	2d	0.451
FeRB	2	0.585	2d	0.405
SRB	2	0.161	2d	0.454
cDCE	2	0.692	2d	0.760
VC	2	0.099	2d	0.172
Ethene	2	0.100	2d	0.171

Data	Batch	NRMSE	Batch	NRMSE
Chloride	3	0.039	3d	0.059
Fe(II)	3	0.738	3d	0.469
Sulfate	3	0.184	3d	0.123
OHRB	3	0.172	3d	0.125
FeRB	3	1.648	3d	0.598
SRBi	3	0.150	3d	0.154
cDCE	3	0.081	3d	0.426
VC	3	0.053	3d	0.217
Ethene	3	0.034	3d	0.218

Data	Batch	NRMSE	Batch	NRMSE
Chloride	4	0.034	4d	0.0452
Fe(II)	4	0.284	4d	0.8047
Sulfate	4	0.163	4d	0.1568
OHRB	4	0.261	4d	0.1239
FeRB	4	0.667	4d	0.6859
SRB	4	0.263	4d	0.1213
cDCE	4	0.650	4d	0.7283
VC	4	0.063	4d	0.0739
Ethene	4	0.063	4d	0.0389

7. References

Abraham, M.H., Whiting, G.S., Fuchs, R., Chambers, E.J., 1990. Thermodynamics of solute transfer from water to hexadecane. J. Chem. Soc. Perkin Trans. 2 2, 291–300. https://doi.org/10.1039/p29900000291

Aeppli, C., Berg, M., Cirpka, O.A., Holliger, C., Schwarzenbach, R.P., Hofstetter, T.B., 2009. SI Influence of mass-transfer limitations on carbon isotope fractionation during microbial dechlorination of trichloroethene. Environ. Sci. Technol. 43, 8813–8820. https://doi.org/10.1021/es901481b

Buttet, G.F., Holliger, C., Maillard, J., 2013. Functional genotyping of Sulfurospirillum spp. in mixed cultures allowed the identification of a new tetrachloroethene reductive dehalogenase. Appl. Environ. Microbiol. 79. https://doi.org/10.1128/AEM.02312-13

Buttet, G.F., Murray, A.M., Goris, T., Burion, M., Jin, B., Rolle, M., Holliger, C., Maillard, J., 2018. Coexistence of two distinct Sulfurospirillum populations respiring tetrachloroethene-genomic and kinetic considerations. FEMS Microbiol. Ecol. 94, 1–11. https://doi.org/10.1093/femsec/fiy018

Chertkov, O., Sikorski, J., Brambilla, E., Lapidus, A., Copeland, A., Glavina Del Rio, T., Nolan, M., Lucas, S., Tice, H., Cheng, J.-F., Han, C., Detter, J.C., Bruce, D., Tapia, R., Goodwin, L., Pitluck, S., Liolios, K., Ivanova, N., Mavromatis, K., Ovchinnikova, G., Pati, A., Chen, A., Palaniappan, K., Land, M., Hauser, L., Chang, Y.-J., Jeffries, C.D., Spring, S., Rohde, M., Göker, M., Bristow, J., Eisen, J.A., Markowitz, V., Hugenholtz, P., Kyrpides, N.C., Klenk, H.-P., 2010. Complete genome sequence of Aminobacterium colombiense type strain (ALA-1T). Stand. Genomic Sci. 2, 280–289. https://doi.org/10.4056/sigs.902116

Cupples, A.M., Spormann, A.M., McCarty, P.L., 2004. Vinyl chloride and *cis*-dichloroethene dechlorination kinetics and microorganism growth under substrate limiting conditions. Environ. Sci. Technol. 38, 1102–1107. https://doi.org/10.1021/es0348647

Elias, D.A., Suflita, J.M., McInerney, M.J., Krumholz, L.R., 2004. Periplasmic Cytochrome c3 of *Desulfovibrio vulgaris* is directly involved in H2-mediated metal but not sulfate reduction. Appl. Environ. Microbiol. 70, 413–420. https://doi.org/10.1128/AEM.70.1.413

Gossett, R.W., Brown, D.A., Young, D.R., 1983. Predicting the Bioaccumulation of Organic Compounds in Marine Organisms using Octanol / Water Partition Coefficients. Mar. Pollut. Bull. 14, 387–392.

Heidelberg, J.F., Paulsen, I.T., Nelson, K.E., Gaidos, E.J., Nelson, W.C., Read, T.D., Eisen, J. a, Seshadri, R., Ward, N., Methe, B., Clayton, R. a, Meyer, T., Tsapin, A., Scott, J., Beanan, M., Brinkac, L., Daugherty, S., DeBoy, R.T., Dodson, R.J., Durkin, a S., Haft, D.H., Kolonay, J.F., Madupu, R., Peterson, J.D., Umayam, L. a, White, O., Wolf, A.M., Vamathevan, J., Weidman, J., Impraim, M., Lee, K., Berry, K., Lee, C., Mueller, J., Khouri, H., Gill, J., Utterback, T.R., McDonald, L. a, Feldblyum, T. V, Smith, H.O., Venter, J.C., Nealson, K.H., Fraser, C.M., 2002. Genome sequence of the dissimilatory metal ion-reducing bacterium *Shewanella oneidensis*. Nat. Biotechnol. 20, 1118–1123. https://doi.org/10.1038/nbt749

Heidelberg, J.F., Seshadri, R., Haveman, S.A., Hemme, C.L., Paulsen, I.T., Kolonay, J.F., Eisen, J.A., Ward, N., Methe, B., Brinkac, L.M., Daugherty, S.C., Deboy, R.T., Dodson, R.J., Durkin,

A.S., Madupu, R., Nelson, W.C., Sullivan, S.A., Fouts, D., Haft, D.H., Selengut, J., Peterson, J.D., Davidsen, T.M., Zafar, N., Zhou, L., Radune, D., Dimitrov, G., Hance, M., Tran, K., Khouri, H., Gill, J., Utterback, T.R., Feldblyum, T. V, Wall, J.D., Voordouw, G., Fraser, C.M., 2004. The genome sequence of the anaerobic, sulfate-reducing bacterium *Desulfovibrio vulgaris* Hildenborough. Nat. Biotechnol. 22, 554–559. https://doi.org/10.1038/nbt959

Jakobsen, R., 2007. Redox microniches in groundwater: A model study on the geometric and kinetic conditions required for concomitant Fe oxide reduction, sulfate reduction, and methanogenesis. Water Resour. Res. 43. https://doi.org/10.1029/2006WR005663

Jossi, M., Fromin, N., Tarnawski, S., Kohler, F., Gillet, F., Aragno, M., Hamelin, J., 2006. How elevated pCO2 modifies total and metabolically active bacterial communities in the rhizosphere of two perennial grasses grown under field conditions. FEMS Microbiol. Ecol. 55, 339–350. https://doi.org/10.1111/j.1574-6941.2005.00040.x

Kröger, A., Biel, S., Simon, J., Gross, R., Unden, G., Lancaster, C.R.D., 2002. Fumarate respiration of Wolinella succinogenes: Enzymology, energetics and coupling mechanism. Biochim. Biophys. Acta - Bioenerg. 1553, 23–38. https://doi.org/10.1016/S0005-2728(01)00234-1

Liu, C., Zachara, J.M., Gorby, Y.A., Szecsody, J.E., Brown, C.F., 2001. Microbial reduction of Fe(III) and sorption/precipitation of Fe(II) on *Shewanella putrefaciens* strain CN32. Environ. Sci. Technol. 35, 1385–1393. https://doi.org/10.1021/es0015139

Lovley, D.R., Roden, E.E., Phillips, E.J.P., Woodward, J.C., 1993. Enzymatic iron and uranium reduction by sulfate-reducing bacteria. Mar. Geol. 113, 41–53. https://doi.org/10.1016/0025-3227(93)90148-O

Malaguerra, F., Chambon, J.C., Bjerg, P.L., Scheutz, C., Binning, P.J., 2011. Development and sensitivity analysis of a fully kinetic model of sequential reductive dechlorination in groundwater. Environ. Sci. Technol. 45, 8395–8402. https://doi.org/10.1021/es201270z

Murray, A., Maillard, J., Jin, B., Broholm, M., Holliger, C., Rolle, M., 2019. A modeling approach integrating microbial activity, mass transfer, and geochemical processes to interpret biological assays: An example for PCE degradation in a multi-phase batch setup. Water Res. 160, 484–496. https://doi.org/10.1016/j.watres.2019.05.087

Muyzer, G., De Waal, E.C., Uitterlinden, A.G., 1993. Profiling of complex microbial populations by denaturing gradient gel electrophoresis analysis of polymerase chain reaction-amplified genes coding for 16S rRNA. Appl. Environ. Microbiol. 59, 695–700. https://doi.org/0099-2240/93/030695-06$02.00/0

Noguera, D.R., Brusseau, G.A., Rittmann, B.E., Stahl, D.A., 1998. A Unified Model Describing the Role of Hydrogen in the Growth of Desulfovibrio vulgaris under Different Environmental Conditions.

Park, H.S., Lin, S., Voordouw, G., 2008. Ferric iron reduction by *Desulfovibrio vulgaris* Hildenborough wild type and energy metabolism mutants. Antonie van Leeuwenhoek, Int. J. Gen. Mol. Microbiol. 93, 79–85. https://doi.org/10.1007/s10482-007-9181-3

Poulton, S.W., Krom, M.D., Raiswell, R., 2004. A revised scheme for the reactivity of iron (oxyhydr) oxide minerals towards dissolved sulfide. Geochim. Cosmochim. Acta 68, 3703–

3715. https://doi.org/10.1016/j.gca.2004.03.012

Rickard, D., Luther, G.W., 2007. Chemistry of iron sulfides, Chemical Reviews. https://doi.org/10.1021/cr0503658

Ritalahti, K.M., Amos, B.K., Sung, Y., Wu, Q., Koenigsberg, S.S., Löffler, F.E., 2006. Quantitative PCR targeting 16S rRNA and reductive dehalogenase genes simultaneously monitors multiple Dehalococcoides strains. Appl. Environ. Microbiol. 72, 2765–2774. https://doi.org/10.1128/AEM.72.4.2765-2774.2006

Sander, R., 2015. Compilation of Henry's law constants (version 4.0) for water as solvent. Atmos. Chem. Phys. 15, 4399–4981. https://doi.org/10.5194/acp-15-4399-2015

Schneidewind, U., Haest, P.J., Atashgahi, S., Maphosa, F., Hamonts, K., Maesen, M., Calderer, M., Seuntjens, P., Smidt, H., Springael, D., Dejonghe, W., 2014. Kinetics of dechlorination by Dehalococcoides mccartyi using different carbon sources. J. Contam. Hydrol. 157, 25–36. https://doi.org/10.1016/j.jconhyd.2013.10.006

Warneck, P., 2007. A review of Henry's law coefficients for chlorine-containing C1 and C2 hydrocarbons. Chemosphere 69, 347–361. https://doi.org/10.1016/j.chemosphere.2007.04.088

Yu, S., Semprini, L., 2004. Kinetics and modeling of reductive dechlorination at high PCE and TCE concentrations. Biotechnol. Bioeng. 88, 451–464. https://doi.org/10.1002/bit.20260

Zhou, C., Zhou, Y., Rittmann, B.E., 2017. Reductive precipitation of sulfate and soluble Fe(III) by *Desulfovibrio vulgaris*: Electron donor regulates intracellular electron flow and nano-FeS crystallization. Water Res. 119, 91–101. https://doi.org/10.1016/j.watres.2017.04.044